



**HAL**  
open science

## **Patient-Specific Computational Evaluation of Stiffness Distribution in Ascending Thoracic Aortic Aneurysm**

Marzio Di Giuseppe, Solmaz Farzaneh, Massimiliano Zingales, Salvatore Pasta,  
Stéphane Avril

► **To cite this version:**

Marzio Di Giuseppe, Solmaz Farzaneh, Massimiliano Zingales, Salvatore Pasta, Stéphane Avril. Patient-Specific Computational Evaluation of Stiffness Distribution in Ascending Thoracic Aortic Aneurysm. *Journal of Biomechanics*, In press, pp.110321. <10.1016/j.jbiomech.2021.110321>. <hal-03139856>

**HAL Id: hal-03139856**

**<https://hal.science/hal-03139856v1>**

Submitted on 12 Feb 2021

**HAL** is a multi-disciplinary open access archive for the deposit and dissemination of scientific research documents, whether they are published or not. The documents may come from teaching and research institutions in France or abroad, or from public or private research centers.

L'archive ouverte pluridisciplinaire **HAL**, est destinée au dépôt et à la diffusion de documents scientifiques de niveau recherche, publiés ou non, émanant des établissements d'enseignement et de recherche français ou étrangers, des laboratoires publics ou privés.



HAL Authorization

1 **Patient-Specific Computational Evaluation of Stiffness Distribution in Ascending**  
2 **Thoracic Aortic Aneurysm**

3 Marzio Di Giuseppe<sup>1</sup>, Solmaz Farzaneh<sup>2</sup>, Massimiliano Zingales<sup>3</sup>,  
4 Salvatore Pasta<sup>3</sup>, Stéphane Avril<sup>2</sup>

5  
6  
7 <sup>1</sup> Department of Health Promotion, Mother and Child Care, Internal Medicine and Medical  
8 Specialties, University of Palermo, 90128, Palermo, Italy

9 <sup>2</sup> Mines Saint-Etienne, Univ Lyon, Univ Jean Monnet, INSERM, U1059 SAINBIOSE, Saint-  
10 Étienne, 42023, France

11 <sup>3</sup> Department of Engineering, Viale delle Scienze, Ed.8, University of Palermo, 90128,  
12 Palermo, Italy

13  
14  
15  
16  
17  
18 Submitting for Original Article

19  
20  
21  
22 Manuscript word count: 3360 words

23  
24  
25  
26 Corresponding author:

27 Stéphane Avril

28 Univ Lyon, INSERM U1059,

29 Mines Saint-Etienne, SAINBIOSE, F-42023,

30 158 cours Fauriel,

31 42023 SAINT-ETIENNE cedex 2, France

32 Phone: +33477420188

33 Fax : +33477420000

34 Email: avril@emse.fr

35  
36  
37  
38  
39  
40  
41  
42  
43  
44  
45  
46  
47  
48  
49  
50  
51  
52  
53  
54  
55  
56  
57  
58  
59  
60  
61  
62

**Abstract**

Quantifying local aortic stiffness properties in vivo is acknowledged as essential to assess the severity of an ascending thoracic aortic aneurysm (ATAA). Recently, the LESI (local extensional stiffness identification) methodology has been established to quantify non-invasively local stiffness properties of ATAAs using electrocardiographic-gated computed tomography (ECG-gated CT) scans. The aim of the current study was to determine the most sensitive markers of local ATAA stiffness estimation with the hypothesis that direct measures of local ATAA stiffness could better detect the high-risk patients.

A cohort of 30 patients (12 BAV and 18 TAV) referred for aortic size evaluation by ECG-gated CT were recruited. For each patient, the extensional stiffness Q was evaluated by the LESI methodology whilst computational flow analyses were also performed to derive hemodynamics markers such as the wall shear stress (WSS).

A strong positive correlation was found between the extensional stiffness and the aortic pulse pressure ( $R=0.644$  and  $p<0.001$ ). Interestingly, a significant positive correlation was also found between the extensional stiffness and patients age for BAV ATAAs ( $R=0.619$  and  $p=0.032$ ), but not for TAV ATAAs ( $R=-0.117$  and  $p=0.645$ ). No significant correlation was found between the extensional stiffness and WSS evaluated locally. There was no significant difference either in the extensional stiffness between BAV ATAAs and TAV ATAAs ( $Q=3.6\pm 2.5$  MPa.mm for BAV ATAAs vs  $Q=5.3\pm 3.1$  MPa.mm for TAV ATAAs,  $p=0.094$ ).

Future work will focus on relating the extensional stiffness to the patient-specific rupture risk of ATAAs on larger cohorts to confirm the promising interest of the LESI methodology.

**Keywords:** Ascending Thoracic Aortic Aneurysm, Bicuspid Aortic Valve, Extensional Stiffness, Noninvasive Inverse Method, Shear Stress

63

## 64 **Introduction**

65 Ascending thoracic aortic aneurysm (ATAA) is a life-threatening cardiovascular disease,  
66 leading to weakening of the aortic wall and permanent dilation. ATAA affects approximately  
67 10 out of 100,000 persons per year in the general population (Coady et al., 1999), and this  
68 disease is associated with a high risk of mortality and morbidity (Elefteriades and Farkas,  
69 2010). Bicuspid aortic valve (BAV) is a predisposing risk factor to ATAA formation and  
70 development with patients having associated aortopathy on approximately 40% of whole  
71 bicuspid population (Verma and Siu, 2014) and higher rate of aortic dissection compared to  
72 patients with the tricuspid aortic valve (TAV) (Januzzi et al., 2004).

73

74 To avoid aortic complications (i.e. rupture or dissection), the current clinical management of  
75 ATAA is based on strict monitoring of the aneurysm size and elective repair is recommended  
76 when aortic diameter reaches a critical size (Berger et al., 2018). However, aortic size is not  
77 a sufficient predictor of the risk of ATAA failure (Pape et al., 2007). Aortic stiffness is  
78 associated with progressive aortic dilatation and aneurysm formation as shown by imaging  
79 modalities (Longobardo et al., 2017; Teixeira et al., 2012), computational analyses (Farzaneh  
80 et al., 2019a; Martin et al., 2013a; Pasta et al., 2017a) and biomechanical studies (Selvin et  
81 al., 2010; Smoljkic et al., 2017). High aortic stiffness was associated with high rates of  
82 surgical aortic replacement and aortic root dilation in children and adults with connective  
83 tissue disorders (Prakash et al., 2015). In Marfan patients, aortic stiffness proved to be  
84 important in predicting progressive aortic dilatation (Guala et al., 2019; Sulejmani et al.,  
85 2017). A recent study of abdominal aortic aneurysms found that segmental stiffening of the  
86 aorta preceded aneurysm growth and introduced the concept that stiffening may act as an  
87 early mechanism triggering elastin breakdown and aneurysm growth (Raaz et al., 2015).  
88 Imaging based on 4D Flow MRI (Mahadevia et al., 2014), in silico computational modeling  
89 (Mendez et al., 2018; Pasta et al., 2017b) or combination of them (Youssefi et al., 2017)  
90 have confirmed an altered hemodynamic environment in BAV ATAAs with well-functioning or

91 stenotic aortic valve leaflets (van Ooij et al., 2017). The underlying hypothesis is that flow  
92 disturbances induce local wall shear stress (WSS) forces on the dilated aorta, portending to  
93 adverse vascular remodeling by mechanotransduction. This can further lead to changes in  
94 the biomechanical properties of ATAA wall as reflected by an increased stiffness for the  
95 dilated aorta.

96

97 Risk assessment based on the aortic stiffness of the ATAA wall are being developed (Duprey  
98 et al., 2016; Farzaneh et al., 2019b; Martin et al., 2013a). In this way, the quantification of  
99 local elastic properties of the ATAA wall from in vivo data is crucial to establish a reliable  
100 method for estimating the severity of an ATAA (Mousavi and Avril, 2017; Rooprai et al.,  
101 2019). Most importantly, new strategies of risk assessment should be accurate and  
102 compatible with clinical time framework. For that purpose, the in vivo non-invasive  
103 identification of aortic stiffness would be essential for clinicians to improve the clinical  
104 decision making process. Recently, Farzaneh et al. (Farzaneh et al., 2019a) have presented  
105 a novel methodology, namely the LESI (local extensional stiffness identification)  
106 methodology, to non-invasively quantify local stiffness properties on the basis of ECG-gated  
107 CT scans and brachial arm pressure. The interrelationship between the obtained local  
108 stiffness with other established markers of aortic function remains unclear and this currently  
109 limits the methodology's potential impact. The aim of the current study was to determine the  
110 most sensitive markers of local ATAA stiffness estimation with the hypothesis that direct  
111 measures of local ATAA stiffness could better detect the high-risk patients. First, the patterns  
112 of extensional stiffness obtained by the LESI methodology in a cohort of 30 patients with  
113 ATAAs and different aortic valve phenotypes were analyzed. Then, the association of  
114 stiffness with demographic data and computationally derived wall shear stress (WSS) was  
115 investigated.

116

117

118

119

## 120 **Methods**

### 121 ***Study Population***

122 After internal review board approval and informed consent, 30 patients (12 BAV and 18 TAV)  
123 referred for aortic size evaluation by electrocardiographic-gated computed tomography  
124 (ECG-gated CT) were enrolled. Table 1 shows demographic data of the patient population as  
125 well as aortic diameter. For all patients, ECG-gated CT scans were performed after  
126 intravenous injection of contrast agent to improve image quality. Imaging was carried out on  
127 a GE VCT 64-channel scanner (GE Medical Systems, Milwaukee, Wisconsin), with gantry  
128 rotation velocity of 0.5 m/s and spiral pitch of 0.984. Retrospective reconstruction of images  
129 was performed to obtain images at cardiac phases corresponding to both end-diastole and  
130 end-systole at the resolution of 512 x 512 and slice thickness of 0.625 mm. Prior to imaging,  
131 diastolic and systolic blood pressures were measured by brachial sphygmomanometer for  
132 each patient.

133

### 134 ***Images Analysis***

135 For each patient, segmentation of ECG-gated CT images was performed at both diastolic  
136 and systolic phases using Mimics v20 (Materialise, Leuven, BE). Specifically, semi-automatic  
137 threshold-based segmentation of the aortic lumen was performed to obtain a point cloud of  
138 ATAA geometries. The same smoothing factor was applied to all phases. The three-  
139 dimensional (3D) surface of the aorta was generated for each phase and exported as STL  
140 file. Then, 3D aortic surfaces reconstructed at both cardiac phases were cut by identical  
141 cross-sectional planes in Rhinoceros (Robert McNeel & Associates, Seattle, USA) to define a  
142 domain of the aorta larger than the final segment of interest. A set of nodes was defined  
143 across each reconstructed aortic geometry, with the requirement that a node represented the  
144 position of the same material point at each phase of the cardiac cycle. For this, it was  
145 essential to reconstruct a structural mesh for all phases with an identical number of elements  
146 and nodes. The Vascular Modeling Toolkit (VMTK, Orobix, Bergamo, Italy; [www.vmtk.org](http://www.vmtk.org))

147 (Antiga and Steinman, 2004) was employed to generate the structural mesh from STL files.  
 148 The extracted data from VMTK were postprocessed in MATLAB to extract an accurate mesh  
 149 using the longitudinal and circumferential metrics obtained from VMTK. A structural mesh  
 150 composed of 3871 quadrilateral shell elements, 49 along the circumferential direction and 79  
 151 along the longitudinal direction, was defined on the template geometry. Each node of the  
 152 structural mesh was related to assumedly the same material points for systole and diastole  
 153 phases.

154 The LESI methodology for calculating the extensional stiffness was described by Farzaneh et  
 155 al. (Farzaneh et al., 2019a). In brief, local principal strain components ( $\varepsilon_1$  and  $\varepsilon_2$ ) were  
 156 deduced by computing the spatial gradients of displacements between diastolic and systolic  
 157 configurations. Although the aortic tissue is globally anisotropic and nonlinear, its mechanical  
 158 behavior was linearized in the range of strains induced by pressure variations between  
 159 diastole and systole, and anisotropic effects were neglected in this range. The local principal  
 160 stress components ( $\tau_1^0$  and  $\tau_2^0$ ) were derived by finite-element analysis (FEA) performed on  
 161 the ATAA diastolic geometry using average blood pressure evaluated over the cardiac cycle  
 162 (Joldes et al., 2016). To obtain radii of curvature ( $r_1^0$  and  $r_2^0$ ) and their variations ( $\Delta r_2$  and  $\Delta r_1$ )  
 163 fast and efficiently, a method based on the principle of virtual work was developed, as  
 164 previously introduced in Bersi et al. (Bersi et al., 2016).

165 Finally it was possible, for each element, to relate the extensional stiffness to the pulsed  
 166 pressure  $\Delta P$  such as:

$$167 \quad Q = \frac{\Delta P + \frac{\tau_1^0 \Delta r_1}{(r_1^0)^2} + \frac{\tau_2^0 \Delta r_2}{(r_2^0)^2}}{\frac{\varepsilon_1 + \nu \varepsilon_2}{r_1^0} + \frac{\nu \varepsilon_1 + \varepsilon_2}{r_2^0}}$$

168 In the current study we used the concept of “extensional stiffness” (intensive property) which  
 169 equals the material stiffness times the thickness and whose dimension is MPa.mm.

170 The aortic thickness could not be measured accurately due to the limited spatial resolution of  
 171 CT.

172 Once LESI results were obtained for each patient, the average extensional stiffness was  
173 evaluated in each of the four quadrants, including the major, minor, anterior and posterior  
174 regions (Fig.1).

175

### 176 ***Computational Flow Analysis***

177 Computational flow modeling was applied to study ATAA hemodynamics at systolic peak  
178 when the aortic valve is supposedly fully open (D'Ancona et al., 2013). For each patient, the  
179 fluid domain of ATAA geometry at end-systole was meshed with unstructured tetrahedral  
180 elements with size of 0.1 mm. The blood was assumed as a non-Newtonian incompressible  
181 fluid (density of 1060 kg/m<sup>3</sup> and viscosity of 0.00371 Pa\*s) adopting the Carreau model  
182 (Khanafar et al., 2006; Leuprecht and Perktold, 2001). The solution was obtained with  
183 FLUENT v18 (ANSYS Inc., Canonsburg, PA) using the SIMPLE algorithm for the pressure-  
184 velocity coupling and second order accurate discretization scheme. To include patient-  
185 specific hemodynamics conditions, the transaortic jet velocity evaluated by Doppler  
186 echocardiography was set as the inflow velocity condition at the aortic valve plane. For each  
187 outlet, we first computed the global vascular resistance and arterial compliance of each  
188 patient from echocardiographic measurements and clinical demographic data. Then, these  
189 parameters were used to compute the outflow boundary conditions of a three-element  
190 Windkessel model (comprising proximal resistance, compliance, and a distal resistance)  
191 coupled to each outflow branch. Boundary conditions were adjusted to match brachial artery  
192 pulse pressure.

193 After numerical solution, WSS values were obtained for the entire thoracic aorta, with further  
194 in-depth subanalysis in the ascending thoracic aorta by computing maxima at sinotubular  
195 junction (namely, analysis plane = AA1), proximal (AA2) and mid (AA3) ascending thoracic  
196 aorta for each quadrant (i.e., major, minor, anterior and posterior quadrants).

197

198

199

## 200 **Statistical Analysis**

201 The Rank Sum test was used to assess differences in the extensional stiffness between BAV  
202 ATAAs and TAV ATAAs. One-way Anova, followed by Holm-Sidak post-hoc test for all pair-  
203 wise comparisons, was used to assess differences of extensional stiffness among aortic  
204 quadrants. The association of the extensional stiffness with patient age, aortic pulse  
205 pressure, aortic diameter, WSS, aortic strain and stress was explored by Pearson's  
206 correlation. Statistical analyses were performed using SigmaPlot (Systat Software Inc., San  
207 Jose, California), with statistical significance set at  $p=0.05$  in all cases. Data are shown as  
208 Mean  $\pm$  SEM.

209  
210 In addition, Principal Component Analysis (PCA) was performed for dimensionality reduction  
211 of all data computed for each patient. First two principal components were analyzed to  
212 assess separation of BAV ATAA versus TAV ATAA. The tolerance ellipse based on  
213 Hotelling's T2 at a significance level of 0.05 was calculated and shown in the score plots.  
214 Principal Component Analysis was performed using SPSS software (IBM SPSS Statistics  
215 v.17, New York, NY).

216

## 217 **Results**

218 Table 1 summarizes patient demographic data, systolic and diastolic pressures and aortic  
219 diameter. The distribution of age in BAV ATAAs differs significantly from that of TAV ATAAs  
220 patients ( $50.2 \pm 7.5$  years for BAV ATAAs vs  $64.7 \pm 7.8$  years for TAV ATAAs,  $p<0.01$ ), and  
221 this difference was confirmed by the analysis of the age on a different cohort of 159 patients  
222 (Agnese et al., 2019).

223

224 Fig. 2 and Fig. 3 show representative extensional stiffness and WSS maps obtained by the  
225 LESI methodology and CFD analyses for BAV ATAAs and TAV ATAAs, respectively. There  
226 was no significant difference in the extensional stiffness (Q) between BAV ATAAs and TAV  
227 ATAAs ( $Q=3.6\pm 2.5$  MPa.mm for BAV ATAAs vs  $Q=5.3\pm 3.1$  MPa.mm for TAV ATAAs,

228 p=0.094). Similarly, the mean values of the extensional stiffness did not significantly change  
229 among aortic quadrants (see Fig.4), although many patients had high values of the  
230 extensional stiffness in the minor and anterior quadrants of the ascending aorta.

231

232 The relationship of extensional stiffness as averaged among quadrants with the ascending  
233 aortic diameter and the aortic pulse pressure are shown in Fig.5A and Fig.5B. A strong  
234 positive correlation was found between the extensional stiffness and the aortic pulse  
235 pressure ( $R=0.644$  and  $p<0.001$ ), but was not significant between the extensional stiffness  
236 and the aortic diameter ( $R=0.341$  and  $p=0.065$ ). Interestingly, a significant positive  
237 correlation was found between extensional stiffness and patients age for BAV ATAAs  
238 ( $R=0.619$  and  $p=0.032$ ), but not for TAV ATAAs ( $R=-0.117$  and  $p=0.645$ ) as shown by  
239 Fig. 5C and Fig. 5D. Fig. 5E and Fig. 5F show the relationship of both strain and stress  
240 obtained in the circumferential direction with the average extensional stiffness. The  
241 extensional stiffness was inversely correlated with the circumferential strain ( $R=-0.522$  and  
242  $p=0.00324$ ) and positively with the circumferential stress ( $R=0.474$  and  $p=0.008$ ). Correlation  
243 analysis of extensional stiffness with age (Fig.5C) also revealed that BAV ATAAs can be  
244 divided into two subgroups: 1) patients younger than 50 years old who had a relatively low  
245 extensional stiffness, 2) patients older than 55 years old who had a relatively high  
246 extensional stiffness. All analysis in Fig.5 were also broken down by aneurysm type, results  
247 are reported in Fig.A1.

248

249 Peak systolic WSSs were correlated to the average extensional stiffness for each ascending  
250 aortic level and aortic quadrant. The correlation analysis between extensional stiffness and  
251 WSS values evaluated at proximal ascending thoracic aorta (AA2) appears promising  
252 ( $R=0.343$  and  $p=0.080$  for AA2), but no significant correlation was found between stiffness and  
253 WSS evaluated locally for Major, Minor and Anterior quadrants. For the Posterior quadrant a  
254 correlation was identified although the obtained p-value was very close to the threshold

255 ( $p=0.05$ ) and a low coefficient was obtained. Results are presented in Fig.6. All analysis were  
256 also broken down by aneurysm type, results are reported in Fig.A2.

257

258 A PCA based on patient's age, aortic diameter, aortic pulse pressure, extensional stiffness  
259 and WSS showed no separation of BAV ATAAs from TAV ATAAs (see Fig. 7). However, the  
260 loading plot revealed that the most important variables responsible for differences between  
261 BAV ATAAs and TAV ATAAs are the pulsed pressure and the patient's age.

262

## 263 **Discussion**

264 This study aimed to investigate the patterns of extensional stiffness from in vivo dynamic  
265 imaging of ATAAs and to evaluate potential correlations with clinical data and blood shear  
266 forces. The extensional stiffness did not show any significant difference between BAV ATAAs  
267 and TAV ATAAs. This supports recent evidence and observations for which there should be  
268 no distinction in the surgical management of BAV patients versus TAV patients (Agnese et  
269 al., 2019). Recently, we performed equibiaxial mechanical testing on ascending aortic tissues  
270 with either BAV or TAV (Di Giuseppe et al., 2019) and found no difference in the mean  
271 values of the aortic tissue stiffness between BAV ATAAs and TAV ATAAs as reported here.  
272 However, other groups who performed mechanical testing on ascending aortic tissues found  
273 differences in the mean values of the aortic tissue stiffness between BAV patients and TAV  
274 patients (Choudhury et al., 2009; Duprey et al., 2010; Okamoto et al., 2002; Pham et al.,  
275 2013; Pichamuthu et al., 2013). We did not measure the extensional stiffness in non  
276 aneurysmatic subjects as healthy subjects cannot undergo CT scans. However the stiffness  
277 of healthy aortas was measured by a variety of other techniques in the literature and values  
278 in a range between 150 kPa and 1000 kPa were reported, with ATAA exhibiting generally a  
279 higher stiffness than healthy aortas (Azadani et al., 2013; Walraevens et al., 2008).

280

281 The correlation of patients' age with the extensional stiffness obtained by the LESI  
282 methodology was strongly affected by the valve phenotype. For TAV patients, the

283 extensional stiffness did not vary with the patient age but increased with the age of BAV  
284 patients. This is likely a consequence of the significant difference in the age of BAV versus  
285 TAV patients. Indeed, TAV ATAAs were older than 50 years while most of patients with BAV  
286 were <50 years. We also found that BAV ATAAs can be divided into two subgroups: 1)  
287 patients younger than 50 years old who had a relatively low extensional stiffness, 2) patients  
288 older than 55 years old who had a relatively high extensional stiffness. Martin et al. (Martin et  
289 al., 2013b) showed that the biomechanical properties of dilated ascending aorta change  
290 between 50 and 60 years, and this could explain either the difference in the extensional  
291 stiffness of two subgroups of BAV ATAAs or the lack of correlation between the extensional  
292 stiffness and patient age for TAV ATAAs.

293

294 As expected, no significant correlation was found between extensional stiffness and shear  
295 stress for Major, Minor and Anterior quadrant, thereby suggesting there is no direct link  
296 between hemodynamics and biomechanical properties of ATAA wall. For the posterior  
297 quadrant, instead, a significant correlation was observed.

298

299 The extensional stiffness was significantly correlated with both the pulsed pressure and the  
300 circumferential strain and stress. Although these variables are directly involved in the  
301 derivation of the aortic stiffness in the LESI methodology, these significant correlations can  
302 also be interpreted with physiological principles.

303 Relations between the aortic stiffness and the pulsed pressure have been known for  
304 decades. Indeed, as the aorta becomes stiffer, the central pulsed pressure is higher due to  
305 the increase in the pulse wave velocity and the early return of reflected waves to the heart  
306 from following junctions (Fung, 1998). In a young and healthy aorta, the reflected wave tends  
307 to hit the aortic root during diastole, serving to increase diastolic pressure and hence  
308 improving perfusion of coronary arteries. In aged and stiffened aortas, the reflected hits the  
309 aortic root earlier, increasing the systolic pressure and decreasing the diastolic one. The  
310 amplitude of reflected waves increases as the arterial stiffness increases, further augmenting

311 central systolic pressure (Chirinos and Segers, 2010a, b; Fung, 1998; Laurent et al., 2005;  
312 Mackenzie et al., 2002; O'Rourke and Nichols, 2005). The effects of this supplemental load  
313 onto the aorta, which are direct expressions of the stiffness increase, should be reckoned for  
314 estimating the risk of rupture or dissection of ATAAs.

315 As expected, the extensional stiffness was also significantly correlated to the circumferential  
316 strain since circumferential strains are a direct expression of the aortic stiffness. Stiffening  
317 often triggers degradation and/or loss of a fraction of elastin fibers, leading to a reduction of  
318 the wall extensibility (Sokolis et al., 2012). Another consequence is also a decrease of the  
319 axial stretch of the aorta, producing an increase of the aortic arch curvature named unfolding  
320 (Redheuil et al., 2011). The degradation of protein networks in the extracellular matrix of  
321 ATAAs can be explained by the unbalance between protein synthesis by vascular cells and  
322 protein destruction by matrix metalloproteases (MMPs) (LeMaire et al., 2005). In the cohort  
323 from which this study group was extracted, we found that the expression level of MMP-9 is  
324 altered in BAV ATAAs vs TAV ATAAs (Gallo et al., 2018). The significant correlation between  
325 extensional stiffness and stress is very common for fibrous soft tissues, owing to their  
326 exponential stress-strain curve (García-Herrera et al., 2012). This reflects reorientation and  
327 straightening of collagen bundles upon loading (Sokolis et al., 2006).

328 When analyzing BAV and TAV ATAAs together, the PCA analysis suggested that BAV  
329 ATAAs are likely forming a cluster in the lower quadrants of the multivariate score plot in the  
330 direction of the loading associated to patient age. This is not surprising because BAV  
331 patients are known to commonly develop ATAA at younger age than TAV (Agnese et al.,  
332 2019; LeMaire et al., 2005).

333

### 334 **Limitations**

335 The LESI approach relies on local equilibrium equations as it is based on the principle of  
336 virtual work (Bersi et al., 2016). As for the generalized Laplace's law, the LESI approach  
337 considers the local equilibrium between pressures and tensions in a membrane, indicating  
338 that the aortic wall experience no shear through the thickness. This may not be a realistic

339 assumption in regions near the aortic branches but these were excluded from the analysis.  
340 The peripheral pulsed pressure rather than central aortic pressure was used. However, the  
341 mismatch of aortic compliance between the brachial artery and the aorta should be likely  
342 reduced or even reversed with the advanced age of our patients. The effect of brachial blood  
343 pressure on the extensional stiffness evaluations will be likely minimal in this study.  
344 Validation of in silico modeling has to be established. A large sample size including BAV  
345 ATAAs matched with the age of TAV ATAAs would be ideal to confirm observations.  
346 Unfortunately, we could not compare results with those relative of non aneurysmatic subjects  
347 because healthy control volunteers are not allowed to undertake multiphase gated CT scans  
348 due to x-ray radiations risks. We are trying to extend our methodology to other imaging  
349 modalities (ultrasounds, MRI).

350

## 351 **Conclusions**

352 We evaluated the patterns of extensional stiffness from the in vivo imaging of ATAAs on a  
353 cohort of 30 patients using the LESI methodology. We found no appreciable differences  
354 between BAV and TAV patients. Regional differences appeared marginal due to inter-  
355 individual variability. The correlation of patients' age with the extensional stiffness strongly  
356 depended on the valve phenotype. Strong relationship of the extensional stiffness with the  
357 pulsed pressure was found, supported by biomechanical explanations.

358

## 359 **Acknowledgments**

360 Stéphane Avril is grateful to the European Research Council (ERC grant Biolochanics, grant  
361 number 647067) for financial support. This work was supported by a "Ricerca Finalizzata" grant  
362 from the Italian Ministry of Health (GR-2011-02348129) to Salvatore Pasta, and by grant from  
363 PON FSE-FESR Ricerca Innovazione 2014–2020 to Marzio Di Giuseppe.

364

## 365 **Conflict of interest statement**

366 The authors confirm there are not conflict of interest associated with this publication.

367  
368  
369  
370  
371  
372  
373  
374  
375  
376  
377  
378  
379  
380  
381  
382  
383  
384  
385  
386  
387  
388  
389  
390  
391  
392  
393  
394  
395  
396  
397  
398  
399  
400  
401  
402  
403  
404  
405  
406  
407  
408  
409  
410  
411  
412  
413

## Reference

Agnese, V., Pasta, S., Michelena, H.I., Minà, C., Romano, G.M., Carerj, S., Zito, C., Maalouf, J.F., Foley, T.A., Raffa, G., Clemenza, F., Pilato, M., Bellavia, D., 2019. Patterns of ascending aortic dilatation and predictors of surgical replacement of the aorta: A comparison of bicuspid and tricuspid aortic valve patients over eight years of follow-up. *Journal of Molecular and Cellular Cardiology* 135, 31-39.

Antiga, L., Steinman, D.A., 2004. Robust and objective decomposition and mapping of bifurcating vessels. *IEEE Transactions on Medical Imaging* 23, 704-713.

Azadani, A.N., Chitsaz, S., Mannion, A., Mookhoek, A., Wisneski, A., Guccione, J.M., Hope, M.D., Ge, L., Tseng, E.E., 2013. Biomechanical properties of human ascending thoracic aortic aneurysms. *The Annals of Thoracic Surgery* 96, 50-58.

Bersi, M.R., Bellini, C., Di Achille, P., Humphrey, J.D., Genovese, K., Avril, S., 2016. Novel methodology for characterizing regional variations in the material properties of murine aortas. *Journal of Biomechanical Engineering* 138, 071005.

Borger, M.A., Fedak, P.W.M., Stephens, E.H., Gleason, T.G., Girdauskas, E., Ikonomidis, J.S., Khojnejhad, A., Siu, S.C., Verma, S., Hope, M.D., Cameron, D.E., Hammer, D.F., Coselli, J.S., Moon, M.R., Sundt, T.M., Barker, A.J., Markl, M., Della Corte, A., Michelena, H.I., Elefteriades, J.A., 2018. The american association for thoracic surgery consensus guidelines on bicuspid aortic valve-related aortopathy: full online-only version. *The Journal of Thoracic and Cardiovascular Surgery* 156, e41-e74.

Chirinos, J.A., Segers, P., 2010a. Noninvasive evaluation of left ventricular afterload: part 1: pressure and flow measurements and basic principles of wave conduction and reflection. *Hypertension* 56, 555-562.

Chirinos, J.A., Segers, P., 2010b. Noninvasive evaluation of left ventricular afterload: part 2: arterial pressure-flow and pressure-volume relations in humans. *Hypertension* 56, 563-570.

Choudhury, N., Bouchot, O., Rouleau, L., Tremblay, D., Cartier, R., Butany, J., Mongrain, R., Leask, R.L., 2009. Local mechanical and structural properties of healthy and diseased human ascending aorta tissue. *Cardiovascular Pathology* 18, 83-91.

Coady, M.A., Rizzo, J.A., Goldstein, L.J., Elefteriades, J.A., 1999. Natural history, pathogenesis and etiology of thoracic aortic aneurysms and dissections. *Cardiology Clinics* 17, 615-635.

D'Ancona, G., Amaducci, A., Rinaudo, A., Pasta, S., Follis, F., Pilato, M., Baglini, R., 2013. Haemodynamic predictors of a penetrating atherosclerotic ulcer rupture using fluid-structure interaction analysis. *Interactive Cardiovascular and Thoracic Surgery* 17, 576-578.

Di Giuseppe, M., Alotta, G., Agnese, V., Bellavia, D., Raffa, G.M., Vetri, V., Zingales, M., Pasta, S., Pilato, M., 2019. Identification of circumferential regional heterogeneity of ascending thoracic aneurysmal aorta by biaxial mechanical testing. *Journal of Molecular and Cellular Cardiology* 130, 205-215.

414 Duprey, A., Khanafer, K., Schlicht, M., Avril, S., Williams, D., Berguer, R., 2010. In vitro characterisation  
415 of physiological and maximum elastic modulus of ascending thoracic aortic aneurysms using uniaxial  
416 tensile testing. *European Journal of Vascular and Endovascular Surgery* 39, 700-707.  
417  
418 Duprey, A., Trabelsi, O., Vola, M., Favre, J.-P., Avril, S., 2016. Biaxial rupture properties of ascending  
419 thoracic aortic aneurysms. *Acta Biomaterialia* 42, 273-285.  
420  
421 Elefteriades, J.A., Farkas, E.A., 2010. Thoracic aortic aneurysm: clinically pertinent controversies and  
422 uncertainties. *Journal of the American College of Cardiology* 55, 841-857.  
423 Farzaneh, S., Trabelsi, O., Avril, S., 2019a. Inverse identification of local stiffness across ascending  
424 thoracic aortic aneurysms. *Biomechanics and Modeling in Mechanobiology* 18, 137-153.  
425  
426 Farzaneh, S., Trabelsi, O., Chavent, B., Avril, S., 2019b. Identifying local arterial stiffness to assess the  
427 risk of rupture of ascending thoracic aortic aneurysms. *Annals of Biomedical Engineering* 47, 1038-  
428 1050.  
429  
430 Fung, Y.-C., 1998. *Biomechanics: circulation*. Springer 9, 155.  
431  
432 Gallo, A., Agnese, V., Coronello, C., Raffa, G.M., Bellavia, D., Conaldi, P.G., Pilato, M., Pasta, S., 2018.  
433 On the prospect of serum exosomal miRNA profiling and protein biomarkers for the diagnosis of  
434 ascending aortic dilatation in patients with bicuspid and tricuspid aortic valve. *International Journal of*  
435 *Cardiology* 273, 230-236.  
436  
437 García-Herrera, C.M., Atienza, J., Rojo, F., Claes, E., Guinea, G., Celentano, D.J., García-Montero, C.,  
438 Burgos, R., 2012. Mechanical behaviour and rupture of normal and pathological human ascending  
439 aortic wall. *Medical & Biological Engineering & Computing* 50, 559-566.  
440  
441 Guala, A., Rodriguez-Palomares, J., Dux-Santoy, L., Teixido-Tura, G., Maldonado, G., Galian, L., Huguet,  
442 M., Valente, F., Gutiérrez, L., González-Alujas, T., 2019. Influence of aortic dilation on the regional  
443 aortic stiffness of bicuspid aortic valve assessed by 4-dimensional flow cardiac magnetic resonance:  
444 comparison with Marfan syndrome and degenerative aortic aneurysm. *JACC: Cardiovascular Imaging*  
445 12, 1020-1029.  
446  
447 Januzzi, J.L., Isselbacher, E.M., Fattori, R., Cooper, J.V., Smith, D.E., Fang, J., Eagle, K.A., Mehta, R.H.,  
448 Nienaber, C.A., Pape, L.A., 2004. Characterizing the young patient with aortic dissection: results from  
449 the international registry of aortic dissection (IRAD). *Journal of the American College of Cardiology* 43,  
450 665-669.  
451  
452 Joldes, G.R., Miller, K., Wittek, A., Doyle, B., 2016. A simple, effective and clinically applicable method  
453 to compute abdominal aortic aneurysm wall stress. *Journal of the Mechanical Behavior of Biomedical*  
454 *Materials* 58, 139-148.  
455  
456 Khanafer, K.M., Gadhoke, P., Berguer, R., Bull, J.L., 2006. Modeling pulsatile flow in aortic aneurysms:  
457 effect of non-Newtonian properties of blood. *Biorheology* 43, 661-679.  
458  
459 Laurent, S., Boutouyrie, P., Lacolley, P., 2005. Structural and genetic bases of arterial stiffness.  
460 *Hypertension* 45, 1050-1055.  
461  
462 LeMaire, S.A., Wang, X., Wilks, J.A., Carter, S.A., Wen, S., Won, T., Leonardelli, D., Anand, G., Conklin,  
463 L.D., Wang, X.L., 2005. Matrix metalloproteinases in ascending aortic aneurysms: Bicuspid versus  
464 trileaflet aortic valves. *Journal of Surgical Research* 123, 40-48.  
465

466 Leuprecht, A., Perktold, K., 2001. Computer simulation of non-Newtonian effects on blood flow in large  
467 arteries. *Computer Methods in Biomechanics and Biomedical Engineering* 4, 149-163.  
468

469 Longobardo, L., Carerj, M.L., Pizzino, G., Bitto, A., Piccione, M.C., Zucco, M., Oreto, L., Todaro, M.C.,  
470 Calabrò, M.P., Squadrito, F., Di Bella, G., Oreto, G., Khandheria, B.K., Carerj, S., Zito, C., 2017.  
471 Impairment of elastic properties of the aorta in bicuspid aortic valve: relationship between  
472 biomolecular and aortic strain patterns. *European Heart Journal - Cardiovascular Imaging* 19, 879-887.  
473 Mackenzie, I., Wilkinson, I., Cockcroft, J., 2002. Assessment of arterial stiffness in clinical practice. *Qjm*  
474 95, 67-74.  
475

476 Mahadevia, R., Barker, A.J., Schnell, S., Entezari, P., Kansal, P., Fedak, P.W., Malaisrie, S.C., McCarthy,  
477 P., Collins, J., Carr, J., 2014. Bicuspid aortic cusp fusion morphology alters aortic three-dimensional  
478 outflow patterns, wall shear stress, and expression of aortopathy. *Circulation* 129, 673-682.  
479

480 Martin, C., Sun, W., Pham, T., Elefteriades, J., 2013a. Predictive biomechanical analysis of ascending  
481 aortic aneurysm rupture potential. *Acta Biomaterialia* 9, 9392-9400.  
482

483 Martin, C., Sun, W., Primiano, C., McKay, R., Elefteriades, J., 2013b. Age-dependent ascending aorta  
484 mechanics assessed through multiphase CT. *Annals of Biomedical Engineering* 41, 2565-2574.  
485

486 Mendez, V., Di Giuseppe, M., Pasta, S., 2018. Comparison of hemodynamic and structural indices of  
487 ascending thoracic aortic aneurysm as predicted by 2-way FSI, CFD rigid wall simulation and patient-  
488 specific displacement-based FEA. *Computers in Biology and Medicine* 100, 221-229.  
489

490 Mousavi, S.J., Avril, S., 2017. Patient-specific stress analyses in the ascending thoracic aorta using a  
491 finite-element implementation of the constrained mixture theory. *Biomechanics and Modeling in*  
492 *Mechanobiology* 16, 1765-1777.  
493

494 O'Rourke, M.F., Nichols, W.W., 2005. Aortic diameter, aortic stiffness, and wave reflection increase  
495 with age and isolated systolic hypertension. *Hypertension* 45, 652-658.  
496

497 Okamoto, R.J., Wagenseil, J.E., DeLong, W.R., Peterson, S.J., Kouchoukos, N.T., Sundt, T.M., 3rd, 2002.  
498 Mechanical properties of dilated human ascending aorta. *Annals of Biomedical Engineering* 30, 624-  
499 635.  
500

501 Pape, L.A., Tsai, T.T., Isselbacher, E.M., Oh, J.K., O'Gara P, T., Evangelista, A., Fattori, R., Meinhardt, G.,  
502 Trimarchi, S., Bossone, E., Suzuki, T., Cooper, J.V., Froehlich, J.B., Nienaber, C.A., Eagle, K.A., 2007.  
503 Aortic diameter  $\geq 5.5$  cm is not a good predictor of type A aortic dissection: observations from the  
504 International Registry of Acute Aortic Dissection (IRAD). *Circulation* 116, 1120-1127.  
505

506 Pasta, S., Agnese, V., Di Giuseppe, M., Gentile, G., Raffa, G.M., Bellavia, D., Pilato, M., 2017a. In vivo  
507 strain analysis of dilated ascending thoracic aorta by ECG-gated CT angiographic imaging. *Annals of*  
508 *Biomedical Engineering* 45, 2911-2920.  
509

510 Pasta, S., Gentile, G., Raffa, G., Bellavia, D., Chiarello, G., Liotta, R., Luca, A., Scardulla, C., Pilato, M.,  
511 2017b. In silico shear and intramural stresses are linked to aortic valve morphology in dilated ascending  
512 aorta. *European Journal of Vascular and Endovascular Surgery* 54, 254-263.  
513

514 Pham, T., Martin, C., Elefteriades, J., Sun, W., 2013. Biomechanical characterization of ascending aortic  
515 aneurysm with concomitant bicuspid aortic valve and bovine aortic arch. *Acta Biomaterialia* 9, 7927-  
516 7936.  
517

518 Pichamuthu, J.E., Phillippi, J.A., Cleary, D.A., Chew, D.W., Hempel, J., Vorp, D.A., Gleason, T.G., 2013.  
519 Differential tensile strength and collagen composition in ascending aortic aneurysms by aortic valve  
520 phenotype. *Annals of Thoracic Surgery* 96, 2147-2154.  
521

522 Prakash, A., Adlakhia, H., Rabideau, N., Hass, C.J., Morris, S.A., Geva, T., Gauvreau, K., Singh, M.N., Lacro,  
523 R.V., 2015. Segmental aortic stiffness in children and young adults with connective tissue disorders:  
524 relationships with age, aortic size, rate of dilation, and surgical root replacement. *Circulation* 132, 595-  
525 602.  
526

527 Raaz, U., Zöllner, A.M., Schellinger, I.N., Toh, R., Nakagami, F., Brandt, M., Emrich, F.C., Kayama, Y.,  
528 Eken, S., Adam, M., 2015. Segmental aortic stiffening contributes to experimental abdominal aortic  
529 aneurysm development. *Circulation* 131, 1783-1795.  
530

531 Redheuil, A., Yu, W.-C., Mousseaux, E., Harouni, A.A., Kachenoura, N., Wu, C.O., Bluemke, D., Lima,  
532 J.A.C., 2011. Age-related changes in aortic arch geometry: relationship with proximal aortic function  
533 and left ventricular mass and remodeling. *Journal of the American College of Cardiology* 58, 1262-1270.  
534

535 Rooprai, J., Boodhwani, M., Beauchesne, L., Chan, K.L., Dennie, C., Nagpal, S., Messika-Zeitoun, D.,  
536 Coutinho, T., 2019. Thoracic aortic aneurysm growth in bicuspid aortic valve patients: role of aortic  
537 stiffness and pulsatile hemodynamics. *Journal of the American Heart Association* 8, e010885.  
538

539 Selvin, E., Najjar, S.S., Cornish, T.C., Halushka, M.K., 2010. A comprehensive histopathological  
540 evaluation of vascular medial fibrosis: Insights into the pathophysiology of arterial stiffening.  
541 *Atherosclerosis* 208, 69-74.  
542

543 Smoljkic, M., Fehervary, H., Van den Bergh, P., Jorge-Penas, A., Kluyskens, L., Dymarkowski, S.,  
544 Verbrugge, P., Meuris, B., Vander Sloten, J., Famaey, N., 2017. Biomechanical characterization of  
545 ascending aortic aneurysms. *Biomechanics and Modeling in Mechanobiology* 16, 705-720.  
546

547 Sokolis, D.P., Kefaloyannis, E.M., Kouloukoussa, M., Marinos, E., Boudoulas, H., Karayannacos, P.E.,  
548 2006. A structural basis for the aortic stress–strain relation in uniaxial tension. *Journal of Biomechanics*  
549 39, 1651-1662.  
550

551 Sokolis, D.P., Kritharis, E.P., Giagini, A.T., Lampropoulos, K.M., Papadodima, S.A., Iliopoulos, D.C., 2012.  
552 Biomechanical response of ascending thoracic aortic aneurysms: association with structural  
553 remodelling. *Computer Methods in Biomechanics and Biomedical Engineering* 15, 231-248.  
554

555 Sulejmani, F., Pokutta-Paskaleva, A., Ziganshin, B., Leshnower, B., Iannucci, G., Elefteriades, J., Sun, W.,  
556 2017. Biomechanical properties of the thoracic aorta in Marfan patients. *Annals of Cardiothoracic*  
557 *Surgery* 6, 610.  
558

559 Teixeira, R., Moreira, N., Baptista, R., Barbosa, A., Martins, R., Castro, G., Providência, L., 2012.  
560 Circumferential ascending aortic strain and aortic stenosis. *European Heart Journal - Cardiovascular*  
561 *Imaging* 14, 631-641.  
562

563 van Ooij, P., Markl, M., Collins, J.D., Carr, J.C., Rigsby, C., Bonow, R.O., Malaisrie, S.C., McCarthy, P.M.,  
564 Fedak, P.W., Barker, A.J., 2017. Aortic valve stenosis alters expression of regional aortic wall shear  
565 stress: New insights from a 4-dimensional flow magnetic resonance imaging study of 571 subjects.  
566 *Journal of the American Heart Association* 6, e005959.  
567

568 Verma, S., Siu, S.C., 2014. Aortic dilatation in patients with bicuspid aortic valve. *New England Journal*  
569 *of Medicine* 370, 1920-1929.

570  
571 Walraevens, J., Willaert, B., De Win, G., Ranftl, A., De Schutter, J., Vander Sloten, J., 2008. Correlation  
572 between compression, tensile and tearing tests on healthy and calcified aortic tissues. *Medical*  
573 *Engineering & Physics* 30, 1098-1104.  
574 Youssefi, P., Gomez, A., He, T., Anderson, L., Bunce, N., Sharma, R., Figueroa, C.A., Jahangiri, M., 2017.  
575 Patient-specific computational fluid dynamics—assessment of aortic hemodynamics in a spectrum of  
576 aortic valve pathologies. *The Journal of Thoracic and Cardiovascular Surgery* 153, 8-20. e23.

577

578

579

580

581

582

583

584

585

586

587

588

589

590

591

592

593

594

595

596

597

598

599 **Figure Legends**

600 **Figure 1:** Representation of ATAA: anterior, posterior, major and minor regions are shown in  
601 boxes.

602 **Figure 2:** Representative extensional stiffness maps of 6 patients reconstructed using LESI  
603 methodology for TAV ATAA and BAV ATAA patients.

604 **Figure 3:** Representative wall shear stress maps of 2 patients obtained by CFD analysis for  
605 TAV ATAA and BAV ATAA patients.

606 **Figure 4:** Comparisons of average extensional stiffness of BAV ATAAs and TAV ATAAs  
607 evaluated at different quadrants.

608 **Figure 5:** (A) Correlation between average extensional stiffness and ascending aortic  
609 diameter; (B) correlation between average extensional stiffness and aortic pulse pressure;  
610 (C) correlation between average extensional stiffness and patients' age of BAV ATAAs; (D)  
611 correlation between average extensional stiffness patients' age of TAV ATAAs; (E) average  
612 extensional stiffness vs circumferential strain data with regression curve; (F) correlation  
613 between average extensional stiffness and circumferential stress.

614 **Figure 6:** Correlation between extensional stiffness and peak systolic WSSs evaluated at  
615 proximal ascending aorta from (A) major, (B) minor, (C) anterior and (D) posterior regions.

616 **Figure 7:** Two-dimensional score plots of PC1 versus PC2 with loading showing the main  
617 variables responsible for clustering BAV ATAAs (black dots) from TAV ATAAs (red dots); the  
618 plot shows patient's age, aortic diameter, aortic pulse pressure, extensional stiffness and wall  
619 shear stress. Solid lines represent 95% tolerance ellipse of TAV ATAAs (red color) and BAV  
620 ATAAs (black color).

621 **Figure A1:** Correlation between average extensional stiffness vs circumferential strain data  
622 with regression curve for BAV (A) and TAV (B) patients; correlation between average  
623 extensional stiffness vs circumferential stress for BAV (C) and TAV (D) patients; correlation  
624 between average extensional stiffness vs aortic pulse pressure for BAV (E) and TAV (F)  
625 patients; correlation between average extensional stiffness vs aortic diameter for BAV (G)  
626 and TAV (H) patients.

627 **Figure A2:** Correlation between extensional stiffness and peak systolic WSSs evaluated at  
628 proximal ascending aorta from major, minor, anterior and posterior regions for BAV  
629 (A,C,E,G) and TAV patients (B,D,F,H).

630

631

632

633

634

635

636

637

638

639

640

641

642

643

644

645

646

647

648

649

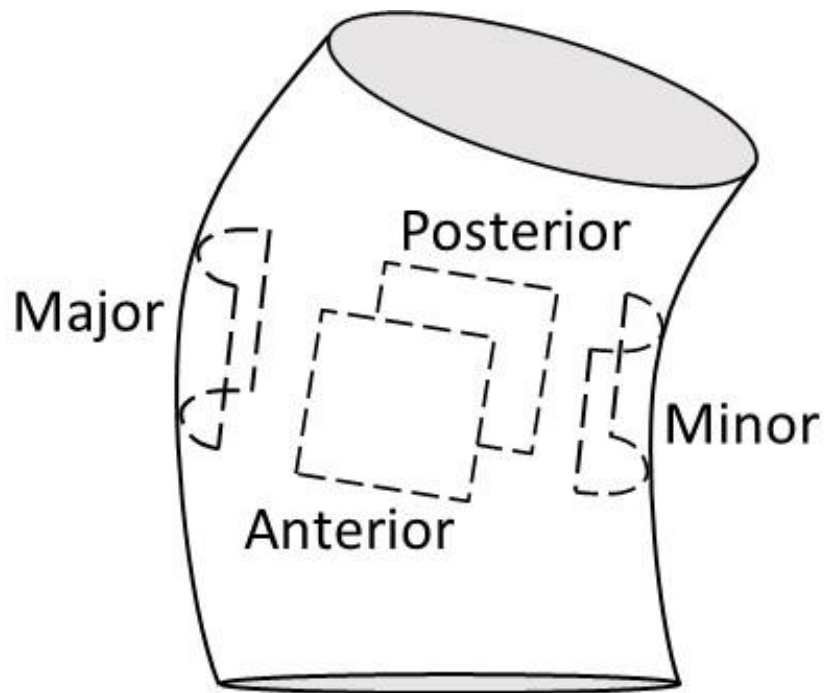
650

651

652

653

654 **Figure 1**



655

656

657

658

659

660

661

662

663

664

665

666

667

668

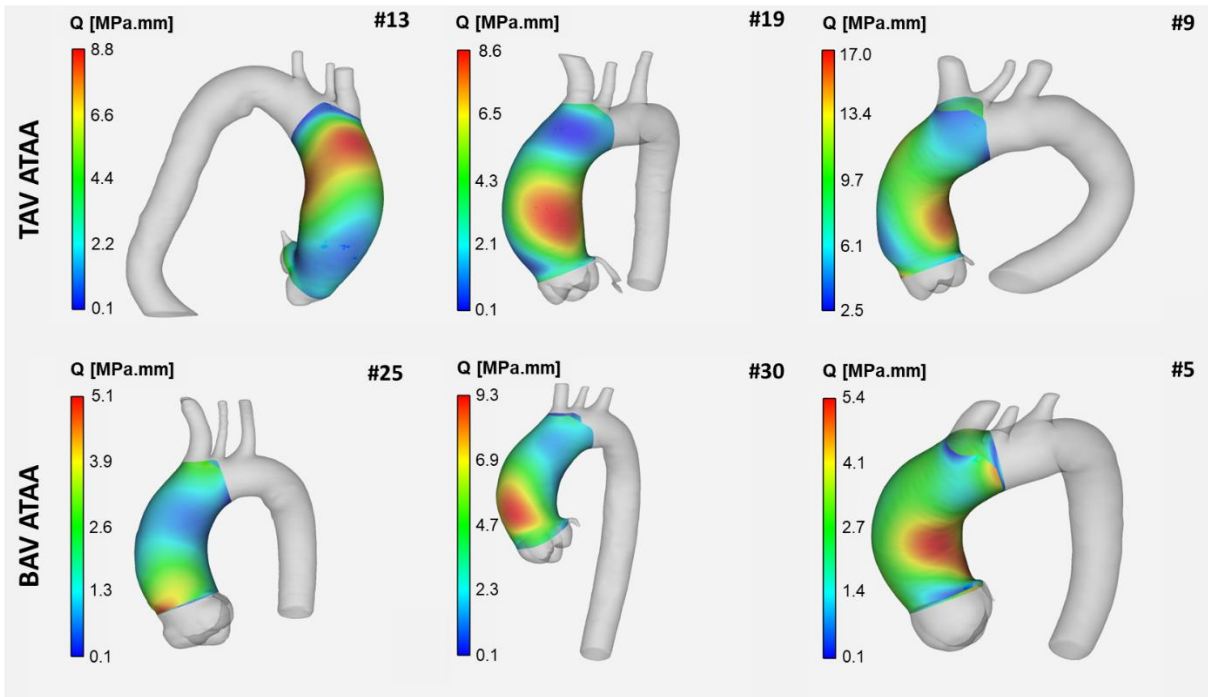
669

670

671

672

673 **Figure 2**



674

675

676

677

678

679

680

681

682

683

684

685

686

687

688

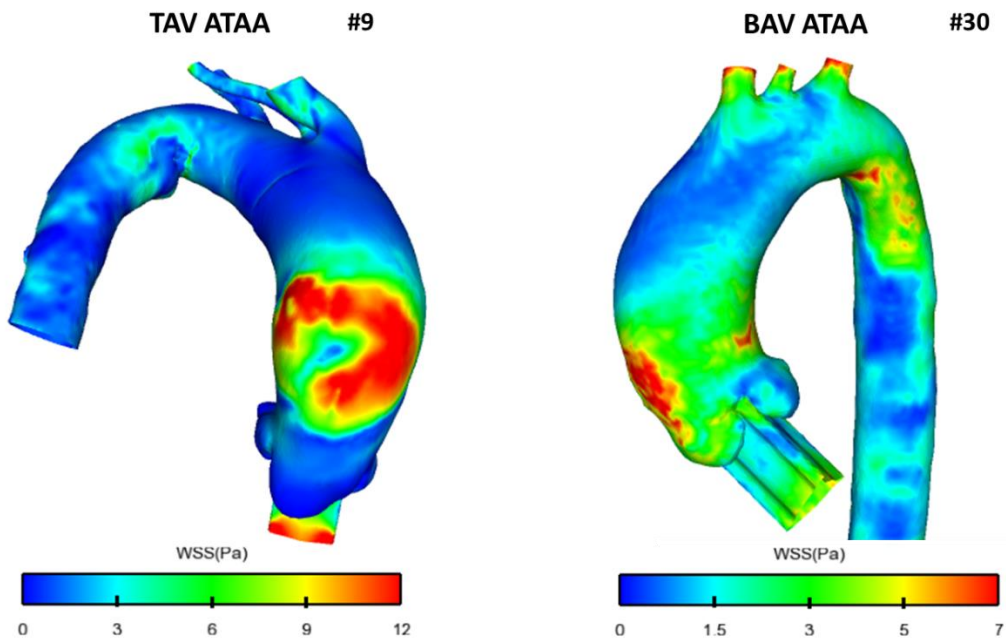
689

690

691

692

693 **Figure 3**



694

695

696

697

698

699

700

701

702

703

704

705

706

707

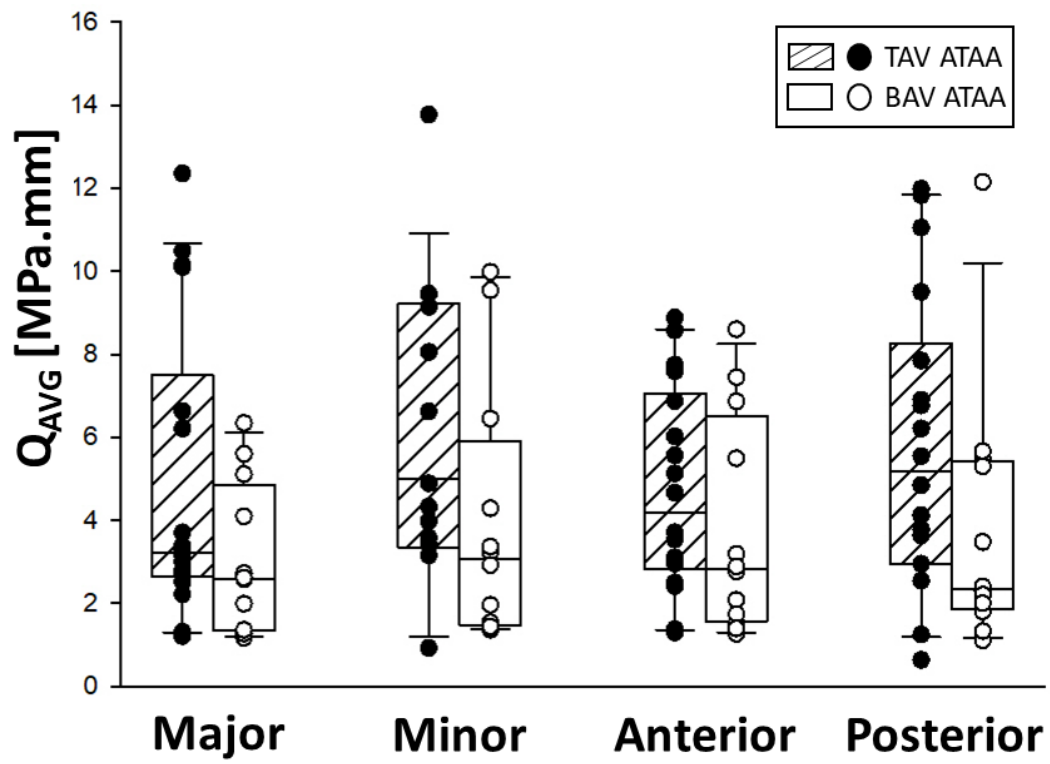
708

709

710

711

712 **Figure 4**



713

714

715

716

717

718

719

720

721

722

723

724

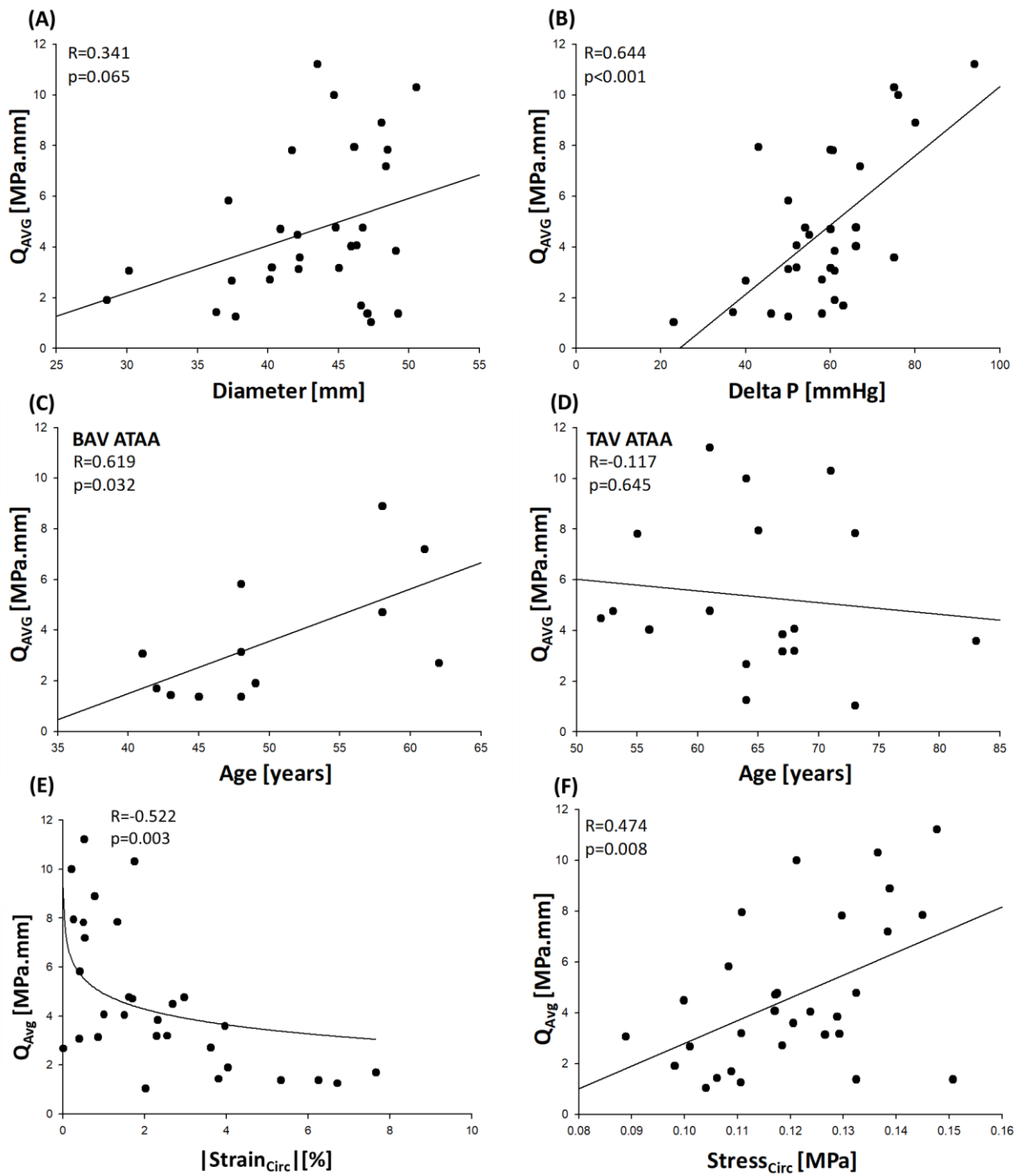
725

726

727

728

729 **Figure 5**



730

731

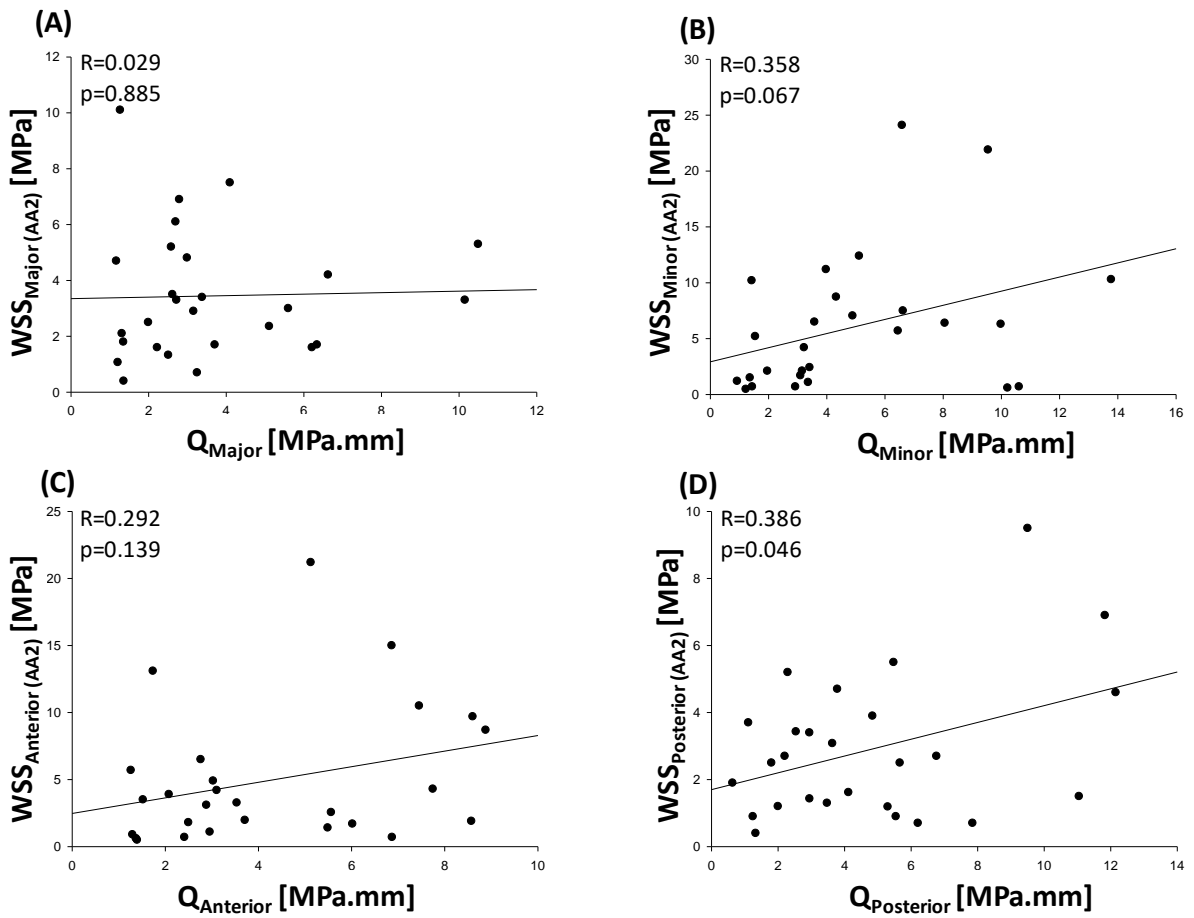
732

733

734

735

736 **Figure 6**



737

738

739

740

741

742

743

744

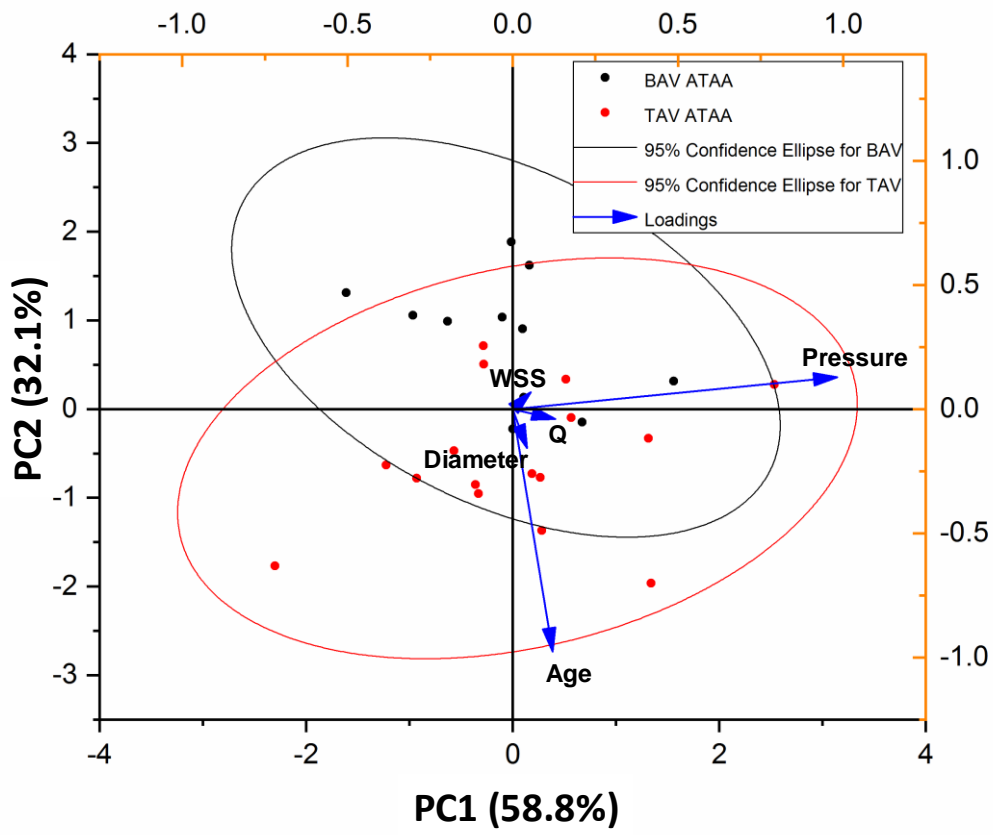
745

746

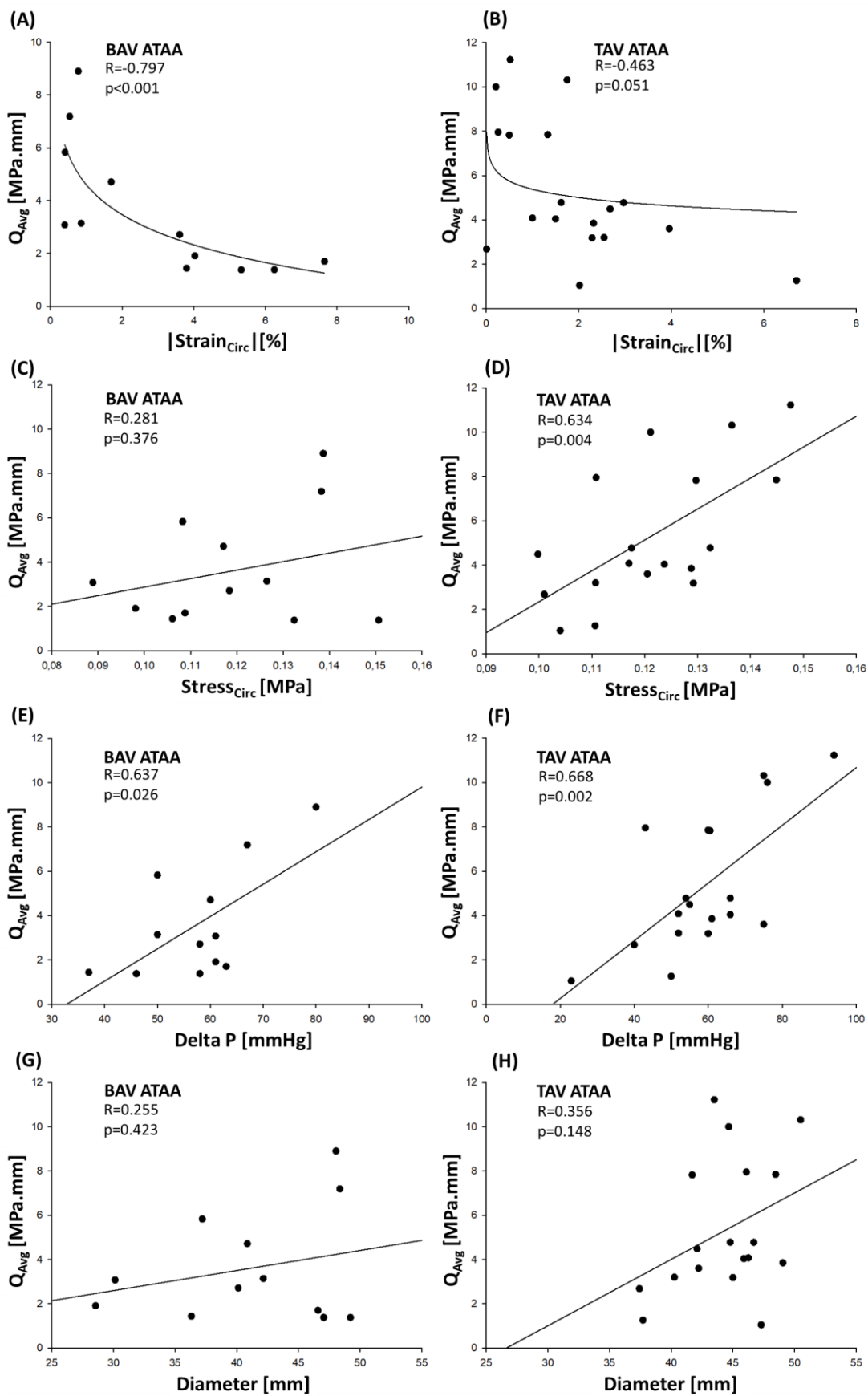
747

748

749 **Figure 7**



750  
751  
752  
753  
754  
755  
756  
757  
758  
759  
760  
761  
762  
763  
764





771 **Table 1:** Demographic and clinical data.

ID	Sex	Valve	Age [years]	Systolic Pressure [mmHg]	Diastolic Pressure [mmHg]	Aortic Diameter [mm]
1	M	TAV	56	140	74	45.9
2	M	TAV	55	136	76	41.7
3	M	BAV	62	135	77	40.13
4	M	BAV	43	125	88	36.32
5	M	BAV	48	135	85	42.15
6	M	TAV	71	145	70	50.5
7	M	BAV	58	150	70	48.04
8	M	TAV	73	100	77	47.3
9	M	TAV	61	180	86	43.5
10	M	TAV	67	136	75	49.05
11	M	TAV	67	140	80	45.01
12	M	TAV	68	122	70	46.27
13	F	TAV	83	150	75	42.23
14	M	TAV	65	116	73	46.1
15	M	TAV	61	136	70	44.8
16	M	BAV	48	130	80	37.2
17	M	BAV	49	136	75	28.56
18	M	TAV	68	129	77	40.27
19	M	TAV	53	126	72	46.7
20	F	TAV	64	144	68	44.67
21	M	TAV	73	144	84	48.47
22	M	BAV	41	136	75	30.13
23	M	BAV	42	131	68	46.59
24	M	TAV	64	120	80	37.43
25	M	BAV	48	148	90	47.05
26	M	TAV	64	130	80	37.71
27	M	BAV	45	124	78	49.21
28	F	BAV	61	144	77	48.36
29	F	TAV	52	125	70	42.1
30	M	BAV	58	136	76	40.86
			58.9±10.4	135.0±13.8	76.5±5.8	43.1±5.4

772

773